Seventh International Conference on CFD in the Minerals and Process Industries
CSIRO, Melbourne, Australia
9-11 December 2009

RESTRICTED REGIONS OF RAYLEIGH-BÉNARD-MARANGONI CONVECTION IN SOLUTE TRANSFER BETWEEN GAS-LIQUID PHASES

Muthasim FAHMY[1], Zhifa SUN[1*] and Tim MOLTENO[1]

[1] Department of Physics, University of Otago, Dunedin 9016, NEW ZEALAND
*Corresponding author, E-mail address: zhifa@physics.otago.ac.nz

ABSTRACT

The limitation of constant concentration boundary condition (described by the penetration theory) at the liquid-solid boundary in evaluation of the critical threshold for Rayleigh and Marangoni instabilities in solute transfer between a gas phase and a liquid phase has been overcome by adopting a non-diffusing boundary condition. Critical thresholds evaluated under this new boundary condition are consistent with penetration predictions within the region where penetration theory is valid. Investigation into the region where penetration theory is no longer valid shows that there is only a limited region within a gas-liquid contactor where convective instability is possible and within this region there is a local maximum of convective intensity, thereby opening up the possibility of enhancing gas-liquid mass transfer with respect to Rayleigh and Marangoni convection.

NOMENCLATURE

A surface convection number
b thickness of gas layer (m)
Bi mass transfer Biot number
C unperturbed concentration of solute in liquid phase (mol m^{-3})
ΔC concentration difference between gas-liquid interface and the bottom liquid-solid boundary (mol m^{-3})
D_g diffusivity of solute in gas phase (m^2 s^{-1})
D_l diffusivity of solute in liquid phase (m^2 s^{-1})
D_s diffusivity of solute in the Gibbs adsorption layer (m^2 s^{-1})
g gravitational acceleration (m s^{-2})
h thickness of liquid layer (m)
k wave number (m^{-1})
k_{cg} gas-phase mass transfer coefficient (m s^{-1})
k_{cl} liquid-phase mass transfer coefficient (m s^{-1})
H Henry law constant for solute (Pa m^3 mol^{-1})
P unperturbed partial pressure of solute in the gas phase (Pa)
Pe Peclet number evaluated using interface velocity
R ideal gas law constant (N m mol^{-1} K^{-1})
Ra Rayleigh number
S surface diffusion number
t dimensionless time
T temperature (K)
u unperturbed velocity (m s^{-1})
Vi surface viscosity number
x dimensionless x-coordinate
z dimensionless z-coordinate

Greek symbols
α solutal expansion coefficient of liquid phase (m^3 mol^{-1})
β dimensionless reverse concentration gradient in the z-direction.
δ Gibbs adsorption depth (m)
κ_s dilational viscosity of Gibbs adsorption layer (N m^{-1} s)
μ viscosity (N m^{-2} s)
μ_s viscosity of the Gibbs adsorption layer (N m^{-1} s)
ν kinematic viscosity (m^2 s^{-1})
ρ density (kg m^{-3})
σ_0 negative of the slope of the curve of surface tension versus solute concentration (N m^2 mol^{-1})

Subscripts
c critical value
g gas phase
i gas-liquid interface
m average value over thickness of gas or liquid layer
0 bottom liquid-solid boundary

Operator
D d/dz

Abbreviations
PEN Penetration theory
NDBB Non Diffusing Bottom Boundary

INTRODUCTION

Heat- and mass-transfer enhancement due to Rayleigh-Bénard (RB) convection and Bénard-Marangoni (BM) convection is a well known phenomenon and continues to be of importance in many engineering applications such as evaporators, absorbers, heat exchangers and falling film reactors (Buffone and Sefiane 2004; Scheid, Kalliadasis, Ruyer-Quil and Colinet 2008).

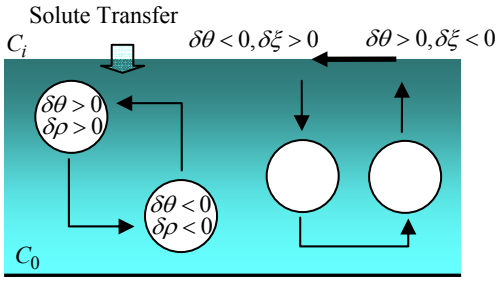

Figure 1: Pictorial representation RBM convection.

Copyright © 2009 CSIRO Australia

RB and BM convection is illustrated in Figure 1, adapted from (Manneville 2006). Gaseous solute diffuses into the top free surface of the liquid layer setting up a concentration gradient along the depth of the layer and hence a corresponding positive density gradient, if the density of the liquid increases with the solute concentration, as assumed for the case shown in Figure 1. The two exaggerated fluid particles on the left of the figure illustrate buoyancy driven convection. If concentration gradient is sufficiently large the diffusion relaxation time can be relatively long compared to the velocity relaxation time. In this case as the particle fluctuates randomly in the bulk, the concentration difference between the particle and its immediate surrounding $\delta\theta = C_p - C_b$ can become negative. The corresponding density difference $\delta\rho = \rho_p - \rho_b$ can therefore momentarily be negative causing an upward buoyancy force that propels the particle into denser liquid reinforcing the buoyancy driving. Similarly a particle that moves from a higher density region to a lower density region can experience a negative buoyancy force that propels the particle further downwards. The buoyancy motions of the upward particle and downward particle can then couple to form continuous convective vortices. The two fluid particles on the right of Figure 1 illustrate surface tension gradient driven convection. Suppose the surface concentration just above the right most fluid particle momentarily increases above the average interface solute concentration and the surface concentration in the region just to the left decreases below the mean interface concentration due to random thermal fluctuation. Then in a liquid for which variation of surface tension with concentration $d\xi / dC$ is negative, the decrease in solute concentration results in an increased surface tension and the increase in solute concentration results in a dip in surface tension. Since a liquid cannot sustain a surface stress, the fluid at the interface moves from the region of lower surface tension to the region of higher surface tension. Fluid continuity means that associated with this surface motion is a pulling up of fluid with a lower concentration into the region where the concentration increased, reinforcing the original concentration gradient, thereby causing sustained fluid vortices.

The classical analyses of systems which simultaneously exhibit the Rayleigh effect and the Marangoni effect, referred to as the Rayleigh-Bénard-Marangoni (RBM) problem (Nield 1964; Palmer and Berg 1973; Lebon and Cloot 1982) to determine the critical threshold of convection are not directly applicable to the practically important two-phase flow systems. By incorporating non-linear velocity profiles (Byers and King, 1967) and assuming a penetration concentration profile (Bird, Stewart and Lightfoot, 1960), Sun and Fahmy (2006) modified the linear analyses due to Nield (1964), Gummerman and Homsy (1974) and Davis and Choi (1977) to be applicable to two-phase parallel flow solute transfer systems which also incorporated the effects of mass and momentum transfer in the Gibbs adsorption layer which were treated separately by previous authors (Scriven and Sternling 1962; Berg and Acrivos 1965; Brian 1971; Brian and Ross 1972). The central prediction of this analysis was that the critical threshold for RBM convection decreases along the downstream flow direction (or with gas-liquid contact time) and therefore convection would begin at the exit end of the gas-liquid contactor and would travel upstream as the mass transfer driving force ΔC was increased. These predictions were qualitatively confirmed via schlieren observation over short contact lengths that guaranteed the applicability of the penetration theory (Sun and Fahmy 2006).

The main limitation of Sun and Fahmy's (2006) analysis of the two-phase flow system is that beyond a non-dimensionalised downstream distance of approximately $x/Pe = 0.03$, the concentration gradient at the liquid-solid boundary is no longer zero as would be required by the physical system having a solid bottom boundary through which no diffusion can take place. In this paper we extend our previous theories to remove this limitation by incorporating a concentration profile consistent with the non-diffusing liquid-solid boundary and making corresponding modification to the linear analysis of the RBM problem, and show how this can lead to a restricted region in the gas-liquid contact channel where RBM convection is possible thereby raising the possibility of optimising RBM enhanced solute transfer between two phase flows.

MODEL DESCRIPTION

The physical system investigated in this paper is shown schematically in Figure 2.

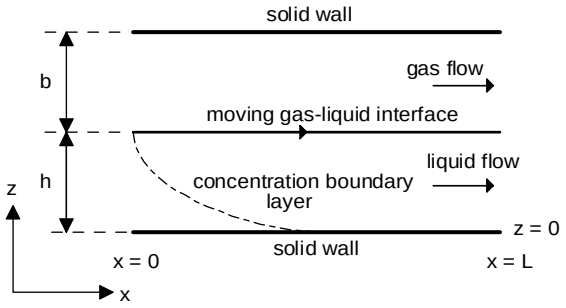

Figure 2: Schematic diagram of the physical system.

In Figure 2, a solute absorption (or desorption) process in a gas-liquid contactor is considered. As shown in this figure, a thin liquid layer of thickness h, with an initial solute concentration of C_0, enters at the inlet ($x = 0$) coming into contact with a gas layer of thickness b containing the solute and an undissolvable gas. If the concentration of two phases at the inlet is uniform, concentration boundary layers would develop as illustrated in Figure 2 for only the liquid phase. The diffusion process within the liquid phase would then be governed by (Byers and King 1967),

$$u_l \partial_t C = \partial_{zz} C \tag{1}$$

At $t = 0$,

$$C(z,t) = C_0 \tag{2}$$

At $z = 1$,

$$C = C_i \tag{3}$$

At $z = 0$,

$$\partial_z C = 0 \tag{4}$$

Copyright © 2009 CSIRO Australia

The above equations are non-dimensionalised with scales h for distance, h^2/D_l for time and $\Delta C=C_0-C_i$ for concentration, and has the solution (Debnath 2004),

$$\frac{C(z,t)-C_0}{C_i-C_0} = \sum_{n=0}^{\infty}(-1)^n\left[\operatorname{erfc}\left(\frac{2n+1-z}{\sqrt{4t}}\right)+\operatorname{erfc}\left(\frac{2n+1+z}{\sqrt{4t}}\right)\right] \quad (5)$$

where n is an integer. Corresponding to the system shown in Figure 2, $t = x/Pe$ in equations (1), (2) and (5).

Defining the reverse concentration gradient as $\beta = -dC/dz$, the following non-dimensionalised and linearised equations have been obtained for the perturbed state of the system,

$$\left(D^2-k^2\right)^2 W(z)-Rak^2\Theta(z)=0 \quad (6)$$

$$\left(D^2-k^2\right)\Theta(z)+\beta(x,z)W(z)=0 \quad (7)$$

At $z = 0$

$$W(z)=DW(z)=D\Theta(z)=0 \quad (8)$$

At $z = 1$,

$$W(z)=0 \quad (9)$$

$$D\Theta(z)-A\,DW(z)=-\left(Bi+k^2S\right)\Theta(z) \quad (10)$$

$$D^2W(z)+k^2Vi\,DW(z)=-k^2Ma\,\Theta(z) \quad (11)$$

Equations (6) and (7) are obtained from the momentum and solute mass balance equations by assuming that perturbation of velocity and concentration can be expanded into normal modes of the form $\mathbf{u}=\mathbf{U}(z)\exp\left[i\left(k_x x+k_y y\right)\right]$ and $\theta=\Theta(z)\exp\left[i\left(k_x x+k_y y\right)\right]$, where $\mathbf{u}=[u,v,w]$, $\mathbf{U}=[U,V,W]$ and $k^2=k_x^2+k_y^2$. Equations (8) and (9) describe the non-diffusing rigid bottom boundary conditions and the non-deformable free surface boundary condition respectively. Equations (10) and (11) arise from a momentum balance and mass balance in the Gibbs adsorption layer at the free interface.

The main difference between the equations above and the equations (37)-(43) established by Sun and Fahmy (2006) is the last relation in equation (8), which describes the non-diffusing boundary investigated in the present paper. The non-dimensional groups in equations (6) through (11) are defined as,

Rayleigh number:

$$Ra=\frac{g\alpha h^3\Delta C}{\nu_l D_l} \quad (12)$$

Marangoni number:

$$Ma=\frac{\sigma_0 h\Delta C}{\mu_l D_l} \quad (13)$$

Surface convection number:

$$A=\frac{C_i\delta}{h\Delta C} \quad (14)$$

Surface diffusion number:

$$S=\frac{D_s\delta}{h\,D_l} \quad (15)$$

Surface viscosity number:

$$Vi=\frac{\mu_s+\kappa_s}{\mu_l h} \quad (16)$$

Biot number:

$$Bi=\frac{Hk_{cg}h}{RTD_l} \quad (17)$$

In addition, the Peclet number is given by,

$$Pe=\frac{u_i h}{D_l} \quad (18)$$

The Biot number is a function of the non-dimensionalised contact time t or the downstream location x/Pe, the gas to liquid diffusivity ratio D_g/D_l, liquid to gas viscosity ratio μ_l/μ_g and the Henry constant H, and is calculated from equations (33) and (34) of Sun and Fahmy (2006).

RESULTS

Under penetration theory, in the region $x/Pe < 0.03$, the concentration at the bottom liquid-solid boundary is $C(z=0)=C_0$. Consequently, under liquid phase controlled mass transfer, where the interface concentration is approximately fixed at $C_i = P/H$, the system driving force $\Delta C = C_0 - C_i$ is approximately constant. For $x/Pe > 0.03$, the vertical concentration gradient is no longer zero at the bottom liquid-solid boundary and therefore penetration theory no longer applies to the practical case where liquid flow is over a solid non-diffusing boundary, and the concentration profile of equation (5) must be used instead. Figure 3 contrasts the penetration concentration profile with non-diffusing bottom boundary (NDBB) profile of equation (5). In Figure 3, at the inlet ($x/Pe = 0$) of the gas-liquid contactor, C_i is assumed to be equal to unity and C_0 is assumed to be zero. In the limiting case of large x/Pe, the NDBB profile is seen to approach the equilibrium condition where the solute concentration is uniform across the depth of the liquid layer, whereas the penetration profile approaches a constant gradient profile which is physically unsatisfactory.

Figure 4 shows the variation of solute concentration at the bottom liquid-solid boundary using equation (5) and the mass transfer Biot number as a function of dimensionless downstream location.

The curves in Figure 4 have been calculated for the typical operating condition: $D_g/D_l = 5000$; $\mu_l/\mu_g = 50$; $b/h = 1$; $u_g/u_l = 1$; and $m/RT = 0.5$ (Sun and Fahmy 2006).

As indicated in Figure 4, the concentration at the bottom boundary rapidly increases when $x/Pe > 0.03$. Consequently, the absolute values of the system operation Rayleigh and Marangoni numbers decrease with the downstream location or contacting time.

Copyright © 2009 CSIRO Australia

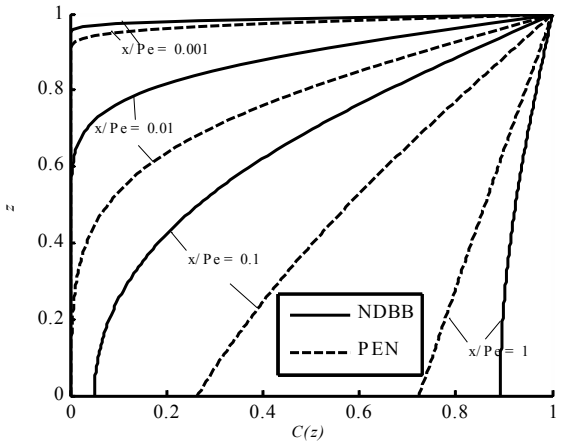

Figure 3: Comparison between penetration and non-diffusing-bottom-boundary concentration profiles for various downstream locations

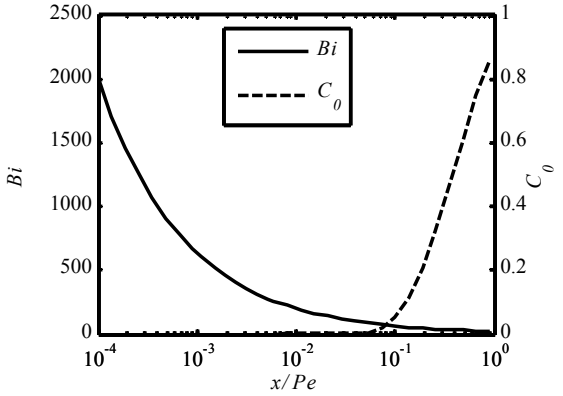

Figure 4: Variation of concentration at the bottom boundary and the mass transfer Biot number with downstream location.

As is evident from equations (12) and (13) we see that Rayleigh and Marangoni numbers are proportional to ΔC and the signs of the Rayleigh and Marangoni numbers depend on whether the fluid physical properties α and σ are positive or negative. For the purpose of illustration, in this paper we have chosen operating parameters such that proportionality constant is positive in equations (12) and (13). The interface concentration non-dimensionalised by taking ΔC as a unit of concentration has been set as $C_i = 1$ and diffusivity of the liquid phase has been taken as a typical value: $D_l = 1\times10^{-9}$ m^2 s^{-1}. With these parameters a unit of dimensionless time corresponds to approximately 1 hour in a typical physical system with a typical organic liquid absorbing or desorbing a solute such as carbon dioxide with a liquid thickness of the order of a few millimetres.

We have solved the eigenvalue problem defined by equations (6) through (11) using a Chebyshev spectral collocation method (Trefethen 2000) to obtain the critical Rayleigh and Marangoni numbers. The pseudospectral method was validated against the method of the variational principles reported in (Sun and Fahmy 2006), under penetration concentration profile conditions. In the following calculations to illustrate the effect of a non-diffusing bottom boundary over parallel flow on the critical threshold for RBM convection over long contact lengths, the effect of Gibbs absorption is not relevant, and therefore the Gibbs numbers *A*, *S* and *Vi* have all been set equal to zero.

For reasons of comparison between the present theory and the penetration model predictions (Sun and Fahmy 2006), we first look at the special case where $Ra = 0$, the Bénard-Marangoni (BM) problem.

Figure 5 shows that for the BM problem, in the region between the gas and liquid inlets to the marginal point ($x/Pe = 0.03$) between a perfectly diffusing wall and an insulating wall, indicated as a black circle point, the penetration theory and the present predictions with non-diffusing bottom boundary are essentially identical. Both profiles thus predict that as we move along the downstream direction the critical threshold for Marangoni convection decreases while the operation Marangoni number remains essentially constant.

Once the critical threshold falls below the operation *Ma*, Marangoni convection begins, and immediately thereafter the system over criticality parameter $(Ma–Ma_c)/Ma_c$ increases approximately linearly with the downstream distance. As the downstream location is further increased, for $x/Pe > 0.03$, the system operation *Ma* is no longer constant but varies as $Ma \propto \left[C_0(x/Pe) - C_i\right]$, producing a local maximum of $(Ma–Ma_c)/Ma_c$ where Marangoni convection is expected to be most intense, and hence where mass transfer rate is a maximum.

Further downstream the system approaches its phase equilibrium conditions with the system operation *Ma* approaching zero. Thus we have a single restricted region along the gas-liquid contactor where Marangoni convection occurs and mass transfer is enhanced. Figure 6 shows how this behaviour can be exhibited in the Rayleigh-Bénard (BM) problem, where $Ma = 0$ and the system operation Rayleigh number now varies as $Ra \propto \left[C_0(x/Pe) - C_i\right]$.

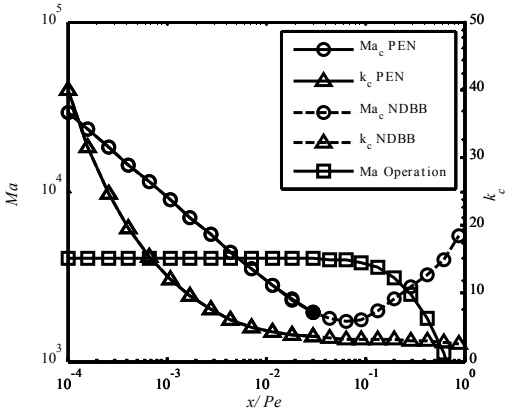

Figure 5: Variation of critical *Ma*, critical *k*, and the system operation *Ma* with downstream location for the BM problem.

As shown in Figure 6 for the RB problem, in the region between the gas and liquid inlets to the marginal point ($x/Pe = 0.03$) between a perfectly diffusing wall and an

Copyright © 2009 CSIRO Australia

insulating wall, the penetration theory and the present predictions with non-diffusing bottom boundary are essentially identical. With further increasing in the downstream distance, the critical *Ra* increases while the system operation *Ra* approaches zero, the phase equilibrium conditions. Similar to the case of the BM problem, we have a single restricted region along the gas-liquid contactor where Rayleigh convection occurs and mass transfer is enhanced.

In Figure 7 we look at the effect of the non-diffusing bottom boundary for the more general case where both Rayleigh and Marangoni convection occur simultaneously.

In a real physical process, even though the system operation *Ra* and *Ma* both decrease with downstream location as shown in **Figure 5** and Figure 6, the ratio *Ma/Ra* is fixed by the fluid physical properties and the process: absorption or desorption (Sun et. al., 2002; Sun and Fahmy, 2006). Thus a straight line, e.g. line P in Figure 7 on which *Ma* = constant × *Ra*, depicts the system operation line on the *Ma*-*Ra* plane. The system follows along the arrow direction on the operation line from an initial entry point I to the final point E at the exit of a gas-liquid contactor. As can be seen in Figure 7, RBM convection can only occur in either the first, second or fourth quadrants. In Figure 7, it is also noted, in particular from the curves of *x/Pe* = 0.03 and *x/Pe* = 0.5, that similar to the behaviour for the cases of the BM problem and the RB problem we have the possibility that critical threshold first decreases and then increases in the general RBM problem. This is explained below.

Along the operation line Q shown in Figure 8, the points 1, 2, 3, 4, and 5 correspond to downstream locations *x/Pe* = 0.03, 0.1, 0.23, 0.5 and 0.8, respectively.

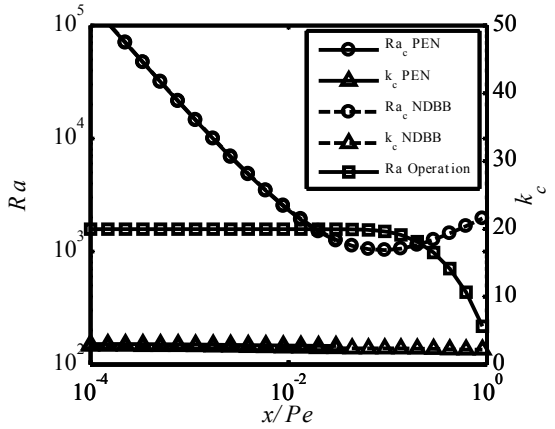

Figure 6: Variation of critical *Ra*, critical *k*, and operation *Ra* with downstream location for the RB problem.

Under typical conditions with a solute such as carbon dioxide and an organic liquid such as methanol with a thickness of a few millimetres, these values of the parameter *x/Pe* correspond to contacting time approximately 2, 5, 15, 30, and 50 minutes, while the critical *Ra*-*Ma* curves at *x/Pe* = 0.001, 0.005, 0.03 and 0.5 corresponds to approximately 0.05, 0.5, 2 and 30 minutes from initial contact respectively. For time less than about 2 minutes, the system operating point remains approximately fixed at point 1 taking approximately 3 minutes to go from point 1 to point 2, while the critical parameters Ra_c and Ma_c, starting from a very large value rapidly approach and then fall below the system operation *Ra* and *Ma* values.

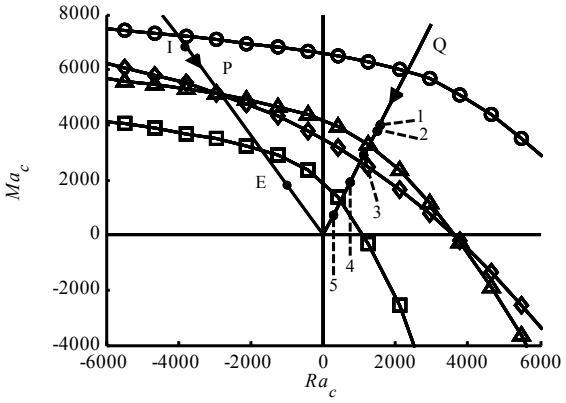

○ ***x/Pe* = 0.001** △ ***x/Pe* = 0.005** □ ***x/Pe* = 0.03** ◇ ***x/Pe* = 0.5**

Figure 7: Variation of critical *Ma* and *Ra* with downstream location for the RBM problem.

Thus the curves shown in Figure 7 indicate that system instability will start within 0.5 minutes of contact. This is typical of critical contact times measured in our laboratory. In the remaining time of contact process, the system operation *Ra* and *Ma* approach the equilibrium value of zero. By the time the system reaches point 4 on the operation line corresponding to approximately 30 minutes, however, the values of the system operation *Ra* and *Ma* have fallen below the critical values and Rayleigh and Marangoni convection subsides.

Therefore, it is the competition between these two effects, the variation of the critical threshold and the variation of the system operation *Ra* and *Ma* that will determine the bounds of the region within the gas-liquid contactor where convective instability can occur. This behaviour is the main difference between the present study and the results reported in figure 8 of Sun and Fahmy (2006), where only the region between the inlet of a gas-liquid contactor and the marginal point (*x/Pe* = 0.03) was investigated.

The critical *Ra*-*Ma* curves in Figure 7 also indicates that for a sufficiently long gas-liquid contactor, the liquid layer may become instable at a location before the exit of the gas-liquid contactor and that the instability would traverse both upstream and downstream with increasing driving force for mass transfer.

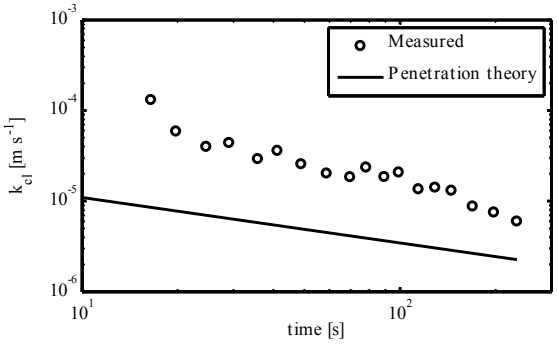

Figure 8: Variation of measured and penetration theory mass transfer coefficient.

Copyright © 2009 CSIRO Australia

The prediction of restricted regions for occurrence of convective instability in gas-liquid contactors with long contact distance has yet to be confirmed experimentally. Nevertheless the collapse of mass transfer enhancement factor, which is defined as the ratio of experimentally measured mass transfer coefficient to that predicted by penetration theory (Brian and Ross, 1972), after a long exposure time has been observed in wetted-wall column (Hozawa et al.,1984). Similar collapse of mass transfer enhancement has also been observed in our laboratory with mass transfer processes in thin quiescent layers, which has a direct correspondence to flow system via the transformation $t = x/Pe$. Such a collapse we observed is illustrated in Figure 8.

It should be noted the reduction in mass transfer rates relative to penetration mass transfer rates is not a viable measure of mass transfer enhancement at a long contact length or time. A more appropriate definition would be with respect to the theoretical instantaneous mass transfer coefficient under the concentration profile of equation (5).

CONCLUSION

Penetration theory is not an adequate basis to evaluate unperturbed concentration profiles in calculations of the critical threshold for the Rayleigh and Marangoni instabilities in solute transfer between a gas layer and a liquid layer between two non-diffusing solid plates when the contact length/time is large. This difficulty has been overcome by enforcing non-diffusing boundary condition to evaluate the unperturbed concentration profile, and correspondingly enforcing non-diffusing boundary conditions in the linearised perturbation equations for the Rayleigh-Bénard-Marangoni problem. Critical thresholds evaluated using the concentration profile satisfying with non-diffusing boundary condition are consistent with those obtained using the penetration concentration profile within the region where penetration theory is valid. Investigation into the region where the penetration theory is no longer valid shows that, both the critical thresholds and the operation Marangoni and Rayleigh numbers are functions of downstream location. Consequently, within certain operation regimes of the system, there can only be a limited region within the gas-liquid contactor where convective instability is possible and within which there is a local maximum of convective intensity, thereby opening up the possibility of optimising gas-liquid contactors with respect to Rayleigh and Marangoni convection enhanced mass transfer, for instance, by paralleling a limited contact area rather than cascading. It has also been pointed out that the reduction in mass transfer enhancement at long exposure observed in a stationary gas-liquid system could be attributed to the competition between system operation Rayleigh and Marangoni numbers and critical thresholds.

REFERENCES

BERG, J.C. and ACRIVOS, A., (1965), "The Effects of Surface Active Agents on Convection Cells Induced by Surface Tension", *Chemical Engineering Science*, **20**, 737-745.

BIRD, R.B., STEWART, W.E. and LIGHTFOOT, E.N. (1960). Transport Phenomena, John Wiley & Sons, Inc.

BRIAN, P.L.T., (1971), "Effects of Gibbs Adsorption on Marangoni Instability", *American Institute of Chemical Engineers Journal*, **17**(4), 756-772.

BRIAN, P.L.T. and ROSS, J.R., (1972), "The Effects of Gibbs Absorption on Marangoni Instability in Penetration Mass Transfer", *American Institute of Chemical Engineers Journal*, **18**(3), 582-591.

BUFFONE, C. and SEFIANE, K., (2004), "Investigation of thermocapillary convective patterns and their role in the enhancement of evaporation from pores", *International Journal of Multiphase Flow*, **30**(9), 1071.

BYERS, C.H. and KING, C.J., (1967), "Gas-Liquid Mass Transfer with a Tangentially Moving Interface: Part I. Theory", *American Institute of Chemical Engineers Journal*, **13**(4), 628-636.

BYERS, C.H. and KING, C.J., (1967), "Gas-Liquid Mass Transfer with a Tangentially Moving Interface: Part II. Experimental Studies", *American Institute of Chemical Engineers Journal*, **13**(4), 637-644.

DEBNATH, L. (2004). Nonlinear Partial Differential Equations for Scientists and Engineers, Birkhäuser.

HOZAWA, M., KOMATSU, N., IMAISHI, N. and FUJINAWA, K., (1984), "Interfacial Turbulence During The Physical Absorption of Carbon Dioxide into Non-Aqueous Solvents", *Journal of Chemical Engineering of Japan*, **17**(2), 173-179.

LEBON, G. and CLOOT, A., (1982), "Buoyancy and Surface Tension Driven Instabilities in Presence of Negative Rayleigh and Marangoni Numbers", *Acta Mechanica*, **43**, 141-158.

MANNEVILLE, P., (2006), "Rayleigh-Bénard convection: Thirty years of experimental, theoretical, and modelling work, in Dynamics of Spatio-Temporal Cellular Structures: Henri Bénard Centenary Review", *Springer Tracts in Modern Physics*, **207,** 41-60.

NIELD, D.A., (1964), "Surface Tension and Buoyancy Effects in Cellular Convection", *Journal of Fluid Mechanics*, **19**, 341-354.

PALMER, H.J. and BERG, J.C., (1973), "Experiments on the Stability of Surfactant Solution Pools Heated From Below", *American Institute of Chemical Engineers Journal*, **19**(5), 1082-1084.

SCHEID, B., KALLIADASIS, S., RUYER-QUIL, C. and COLINET, P., (2008), "Interaction of Three-dimensional Hydrodynamic Thermo capillary Instabilities in Film Flows", *Physical Review E, Statistical, Nonolinear, Soft Matter*, **78**, 066311.

SCRIVEN, L.E. and STERNLING, C.V., (1962), "On Cellular Convection Driven by Surface-Tension Gradients: Effects of Mean Surface Tension and Surface Viscosity", *Fluid Mechanics*, **19**, 321-340.

SUN, Z.F. and FAHMY, M. (2006). Location of Onset of Rayleigh-Bénard-Marangoni Convection in Gas-Liquid Mass Transfer with Two-Phase Flow. Chemeca 2006.

SUN, Z.F. and FAHMY, M., (2006), "Onset of Rayleigh-Bénard-Marangoni Convection in Gas-Liquid Mass Transfer with Two-Phase Flow: Theory", *Industrial and Engineering Chemistry Research*, **45**, 3293-3302.

SUN, Z.F., Yu, K. T., WANG, S. Y., MIAO, Y. Z. (2002) Absorption and Desorption of Carbon Dioxide into and from Organic Solvents: Effects of Rayleigh and Marangoni Instability. *Industrial and Engineering Chemistry Research*, **41**, 1905.

TREFETHEN, L.N., (2000), Spectral Methods in Matlab, Siam.

Copyright © 2009 CSIRO Australia